REVIEW

Check for updates

Biochemical transformations of inorganic nanomedicines in buffers, cell cultures and organisms

Anna L. Neuer, [iD] [a,b] Inge K. Herrmann [iD] [a,b] and Alexander Gogos [iD] ★[a,b]

The field of nanomedicine is rapidly evolving, with new materials and formulations being reported almost daily. In this respect, inorganic and inorganic–organic composite nanomaterials have gained significant attention. However, the use of new materials in clinical trials and their final approval as drugs has been hampered by several challenges, one of which is the complex and difficult to control nanomaterial chemistry that takes place within the body. Several reviews have summarized investigations on inorganic nanomaterial stability in model body fluids, cell cultures, and organisms, focusing on their degradation as well as the influence of corona formation. However, in addition to these aspects, various chemical reactions of nanomaterials, including phase transformation and/or the formation of new/secondary nanomaterials, have been reported. In this review, we discuss recent advances in our understanding of biochemical transformations of medically relevant inorganic (composite) nanomaterials in environments related to their applications. We provide a refined terminology for the primary reaction mechanisms involved to bridge the gaps between different disciplines involved in this research. Furthermore, we highlight suitable analytical techniques that can be harnessed to explore the described reactions. Finally, we highlight opportunities to utilize them for diagnostic and therapeutic purposes and discuss current challenges and research priorities.

Introduction

Over the past 25 years, nanotechnology has received increasing attention in the biomedical field. The design,[1,2] tunability,[3,4] biomedical efficacy,[5] and characterization[6,7] of nanomaterials (NMs) for biomedical applications have been widely studied. In addition to studies on organic nanomaterials, such as liposomes and micelles, detailed studies on inorganic and organic–inorganic composite NMs have been conducted.[8,9] Such materials have been used extensively in applications, as imaging agents,[10–13] in drug delivery systems,[14,15] in radioenhancement therapy,[16–19] and in wound healing.[20–22] They have also been used as theranostic agents (combining diagnostics and therapy)[9,23] due their exclusive and tailorable properties.

Nonetheless, compared to the abundance of nanomedical research, with around 10 000 publications per year, the clinical use of nanomedicines is greatly limited, with only about 200 organic and inorganic nanomedical drugs having entered clinical phases to date.[24] Clinical translation remains challenging[25] due to the oftentimes limited understanding and control over the nanomaterial chemistry during all stages of material life-cycle from stable storage to applications, covering bioavailability and fate within the body, metabolism and ultimately excretion/elimination processes. While many of these aspects have been well-characterized for organic nanomaterials (liposomes and micelles),[26,27] research on the physical and chemical modification and transformation of inorganic NMs within the body is still scarce.[28] Physical and chemical changes in NMs are related to modifications in NM composition and structure, and therefore to modified efficacy and safety profiles. Those factors need to be strictly controlled if NMs are intended for medical use, as NMs might undergo physical and chemical transformations upon interaction with the different chemical environments within the body, such as variations in pH, ion composition, and redox potential. In this context, research on NM stability has mostly focused on NM decomposition and degradation (often monitored as a loss of function over time),[29] as well as on corona formation;[30,31] *i.e.*,

[a]Laboratory for Particles-Biology Interactions, Department of Materials Meet Life, Swiss Federal Laboratories for Materials Science and Technology (Empa), Lerchenfeldstrasse 5, 9014 St. Gallen, Switzerland. E-mail: alexander.gogos@empa.ch; Tel: +41 (0)58 765 78 05
[b]Nanoparticle Systems Engineering Laboratory, Institute of Process Engineering, Department of Mechanical and Process Engineering, ETH Zurich, Sonneggstrasse 3, 8092 Zurich, Switzerland

the formation of secondary (bio-)molecule layers on the NM surface. However, in biomedical research, there is a gap between the number of studies reporting the design of new NMs and those assessing NM fate, including primary reactions and secondary effects. Primary transformations may result in alterations in elemental speciation, crystal structure, material composition and/or morphology of the NM, as well as the generation of secondary nanoparticles. These alterations can have a major impact on the *in vivo* efficacy, toxicity, and fate. The occurrence and impact of such NM transformations have been widely acknowledged and studied in various fields, such as nano-environmental health and safety (nanoEHS),[32–34] catalysis[35] and energy applications.[36–38] However, over the past several years, the importance and relevance of NM transformation have become also recognized by the biomedical field.[39]

In this review, we highlight studies on the transformation of inorganic and organic–inorganic composite NMs (metals, metal-oxides, and metal organic frameworks (MOFs)) that are relevant for various biomedical applications; such applications are realized under cell-free, *in vitro*, *ex vivo*, and *in vivo* conditions. Hereafter, "NMs" refers to inorganic and inorganic–organic composite materials and will be assessed with a focus on chemical transformation, including changes in element speciation, crystal structure, material composition and morphology,[40] as well as the formation of secondary nanoscale phases from the parent material. Studies that solely investigate dissolution are excluded since they have been extensively reviewed elsewhere.[29–31] Additionally, we point to successful measures that protect clinically relevant inorganic NMs from transformation, as well as specific transformations that might be harnessed to endow NMs with additional functionality. Moreover, we provide a comprehensive overview of suitable analytical techniques that can be leveraged to gain insights into the underlying reaction mechanisms for material transformations. Ultimately, a better understanding of potential transformation reactions allows for better safe-by-design approaches and tunable transformation for therapeutic, diagnostic, and elimination purposes.

Application routes for inorganic nanomedicines and associated biological environments

Application routes for inorganic nanomedicines *in vivo* can be divided into four principal categories: (i) oral administration,[41] (ii) inhalation/tracheal administration,[41] (iii) injection (which can further be divided into (iii.a) intravascular[41–46] (IV) (iii.b) direct site[47] and (iii.c) retroorbital[48] injection (which is solely found in rodent studies)), as well as (iv) subcutaneous and transdermal[49–52] application (see Fig. 1A). The route of administration is highly dependent on the intended medical application, the bioavailability, as well as the NM surface chemistry and size.[53] The size and surface chemistry of NM are of paramount importance. As the size decreases, the proportion of

surface atoms becomes increasingly pronounced, which in turn significantly influences the long-term fate of NM, especially under varying pH values and ionic strengths of the environment. The surface chemistry, along with any coatings, can serve dual roles: they can act as protective layers, stabilizing the NM, or they can actively modulate interactions with the surrounding environment. This surface chemistry determines the charge, hydrophobicity, and affinity of the NM, all of which play pivotal roles in how these materials interact with biological systems.[54] The application route defines the local fate of the NM as well as the chemical environment the NM is first exposed to. After oral administration, studied typically with oral gavage in rodents,[41] the NM is exposed to the milieus of the gastrointestinal (GI) tract starting from the stomach, all the way to the small intestine, and then to the large intestine (SI/LI). This involves drastic changes in pH, from pH 1.0–3.0 (stomach) to pH 5.4–7.5 (SI) and pH 6.6–7.4 (LI)[55] (Fig. 1B). Additionally, digestive enzymes may be present, which, again, is strongly dependent on the exact anatomical location. The entire gastrointestinal system is lined by a mucosal layer, separating the cells of the gastrointestinal tract from its contents. In a healthy GI tract, the mucosal layer shields the intestinal cells, to a certain extent, from interactions with ingested nanomaterials. However, disruption of this barrier, *e.g.*, due to inflammatory bowel disease (IBD), has shown altered exposure of the GI to ingested NMs, hence indicating a strong dependence of NM fate on the barrier being intact.[56]

In contrast to oral NM administration, the conditions encountered by NMs *via* inhalation or tracheal administration[41] are distinctly different; the first organ of contact is the lung, with a neutral pH of around 7.0, coated with a mucosal layer that protects it from the external environment. For inhalation or intratracheal exposure, NM uptake into alveolar macrophages and epithelial cells has been reported, with further translocation of NM to the vascular system.[57]

A benefit of injection into blood either intravenously[41–46] (or retroorbitally in rodents[48]), which is favored by most studies, is direct systemic distribution with exposure to a near-neutral pH of 7.1–7.6.[58] Nonetheless, blood (Fig. 1B) is a very complex environment, containing phosphates (0.9–1.5 mmol l^{-1} (ref. 59)), macromolecules (60–80 g l^{-1} (ref. 60)), and a variety of ions (e.g., Ca^{2+}, Cl^-, K^+, Na^+). Unless the GI tract or the lung is the primary target organ for the clinical application of nanomedicine, injections are typically preferable. Intravenous administration gives access to circulation in the blood stream and, therefore, a systemic distribution; however NM fate is heavily influenced by their interaction with the reticuloendothelial system (RES), including the liver, kidneys, and/or spleen, where NMs preferentially accumulate.[42,43,45,48] Depending on the target organ and therapy involved, a direct site injection may have advantages over intravenous administration, achieving a highly defined and concentrated local NM distribution.[47] This is crucial for several therapies, such as NM-enhanced radiotherapy (Hensify®, NBTXR3)[61] and magnetic hyperthermia (MagForce AG, NanoTherm® Therapy)[62,63] of solid tumors.
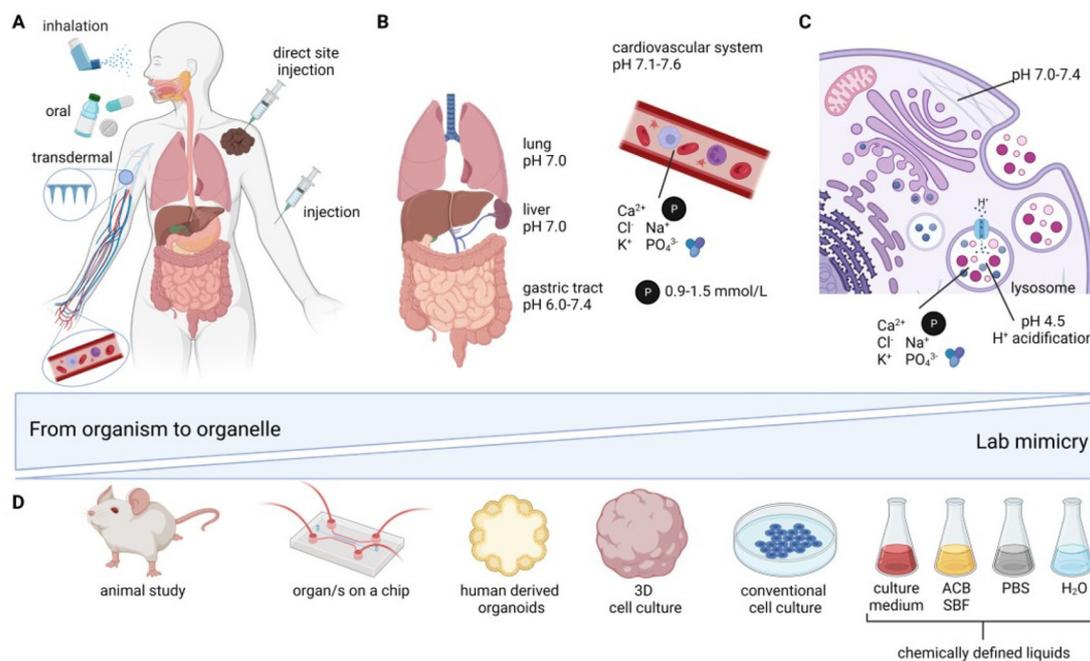
Fig. 1 Application routes for inorganic nanomedicines and associated biological environments (A) in a whole organism, (B) at the organ level with tissue-specific pH values and ion/macromolecule compositions, and (C) in the endosomal–lysosomal cellular uptake mechanism of NMs, with lysosomal-specific composition of ions, macromolecules, phosphate, and pH values. The organism to organelle compartments are juxtaposed to (D) lab mimicries with bar "Lab mimicry" indicating restricted availability, high throughput and simplicity. Ranging from chemically defined liquids (phosphate buffered saline (PBS), artificial compartment buffer (ACB), simulated body fluids (SBF)), in vitro systems to in vivo.

Irrespective of the route of administration, the therapeutic efficacy of almost all NMs relies on the NM uptake by cells.[64] The most relevant cellular uptake mechanism for NM is via endocytosis (Fig. 1C).[64] The NM is taken up by cells from the extracellular space into endosomes with an initial pH of 6.0–6.5.[65] Over the course of endosomal maturation and V-ATPase acidification (H^+ pump), the endosomes mature to late endosomes with a pH value of 5.0–6.0.[65] Further maturation and acidification fully converts the endosomes into lysosomes with a pH of 4.5–5.0,[65–68] corresponding approximately to a 25 μM H^+ concentration, which is roughly 500 times higher than the cytosolic H^+ concentration.[62] Lysosomes (Fig. 1C) are vesicles found in most eukaryotic cells containing a wide variety of enzymes relevant for (bio-) macromolecule degradation. Additionally, lysosomes play a role in cellular processes, such as the secretion of proteins, cell signaling, and metabolic processes.[69] The size of lysosomes varies from 0.1–0.6 μm, and they are containing a diverse set of enzymes (e.g., phosphatases, lipases, proteases, and sulfatases, responsible for different degradation and digestion processes) and ions (0.5 mM Ca^{2+}, 20–140 mM Na^+, 2–50 mM K^+, 60–80 mM Cl^-).[62] All of the aforementioned factors, including phosphates, macromolecules, and ions (Ca^{2+}, Cl^-, K^+, Na^+, H^+), and various combinations of these, add complexity to the biochemical environment that the NM is exposed to. The major challenges when studying transformation in whole organisms include: (i) highly dynamic effects, (ii) multifactorial reactions, as well as (iii) observer bias (i.e., "you only see what you look for"). Even though there is increased focus on

the chemical and physical changes inherent to NM research for biomedical applications, most studies continue to focus on degradation and loss of function and not on primary environment-specific transformation reactions. Therefore, the interaction between complex in vitro or in vivo environments and NMs with associated transformations can currently be considered a "black-box", with native NMs as the input and transformed NMs as the output. However, the underlying reactions are potentially a series of primary/elementary reactions/processes that result in secondary processes, such as degradation, amorphization, and recrystallization. To understand these fundamental processes, it is often essential to carefully simplify the environment to better discern the reaction mechanisms at play. However, such simplified studies should always be complemented by research in more advanced in vitro human models, as well as ex vivo or in vivo models. This approach verifies the occurrence of significant transformations. For example, morphological changes to CuS/CuS-iron oxide NM were first observed in vitro and afterwards confirmed in vivo.[70] Drawing correlations between findings in intricate in vivo scenarios and those in more basic systems will contribute to the safe and sustainable translation of NMs towards clinical trials. As systematic in vivo investigations are time consuming, laborious, and resource intensive, adequate alternatives are needed, not only to reduce the amount of animals sacrificed, but also to unravel primary reaction mechanisms in less complex environments (Fig. 1D). The complexity of the lab systems need to be as defined as possible, with greatly reduced numbers of unknown

variables that mimic single compartments and biological environments, such as lysosomes, blood, and tissue differences. Gradual complexity reduction, from whole *in vivo* organisms to cell-free systems, might be obtained using: (i) *ex vivo*[71,72] and organ-on-a-chip approaches,[73] (ii) mono- or co-cultured 3D *in vitro* models,[74,75] (iii) conventional monolayer *in vitro* cell cultures,[75,76] (iv) cell-free buffer systems, and (v) *in silico* modeling approaches[77] (Fig. 1D).

Nanomaterial transformation: a cascade of primary and secondary reactions

Most studies on NMs for biomedical applications discuss endpoints, such as degradation or loss of function. These endpoints are secondary effects rather than primary/elementary reactions, on which the focus will be placed in the following.

In classical chemical reaction theory, a reaction mechanism has one or more elementary reactions. These reactions consist of only one reaction step and one transition state involving one or more reactants. As previously discussed, the reactions that NMs undergo in model systems are intrinsically complex, not only due to the complexity of the model system and environments the NM's are facing, but also the NM's own complex structure (*e.g.*, MOFs). Here we break down the transformation processes into two main classes: primary and secondary transformation processes. Our aim is to elucidate the black box of NM transformation, and to clarify transformation reaction terminology to produce a starting point in unifying the scientific language of NM transformation. We consider primary processes to be the very first steps in initiating a transformation of the parent material, *i.e.*, a deviation from the material's original chemical, morphological, and/or structural states. Primary processes can be easily differentiated from secondary processes, as secondary processes are the result of one or more sequentially or simultaneously occurring primary processes (primary–secondary-reaction-cascade). We systematically analyzed studies (Table 1) in which primary and secondary processes that involved NMs for biomedical applications were determinable. To give a short example of such a primary–secondary-reaction cascade, the transformation of ZIF-8, a Zn-based MOF, in phosphate buffered saline (PBS) is described as a corrosion reaction of the Zn^{2+} centers with free phosphate groups.[78] The gradual formation of zinc phosphate leads to a release of the organic linker, gradual amorphization, and the loss of the original structure as secondary processes.[78]

Primary chemical reaction mechanisms dependent on the chemical environment

Every biological environment, such as tissue, blood, and cell organelles, can be translated to an environment that drives chemical reactions. From the studies analyzed in Table 1, four main types are identified: hydrolysis, redox reactions, corrosion and complexation. Their relative importance is heavily dependent on the environment and intended application: pH, (mineral) ion composition and concentration, protein and macromolecule composition, as well as irradiation as an external parameter (Fig. 2). All of these parameters initiate specific reaction mechanisms, hereafter termed "primary reactions".

One of the simplest and most widely studied primary reactions is hydrolysis. This reaction is mediated by water and its dissociation products, OH^- and H^+, which react with the original molecule, causing it to break down into smaller molecules. Hydrolysis is an integral reaction in many biological processes, such as food digestion and metabolism, also known as chemical digestion.[103,104] This reaction can be accelerated under basic or acidic conditions and is temperature dependent; however, near-neutral to acidic conditions dominate under normal human physiological conditions, with individual variations in temperature around 37 ± 0.5 °C (Fig. 1).[105] For example, Fe-MIL MOFs, mainly investigated for drug delivery applications, hydrolyzed in water, resulting in cleavage of the metal clusters and the linker into amorphous ferrihydrite ($Fe_2O_3 \cdot 2H_2O$) and its respective linker molecule[97] (Fig. 2A). This reaction was more pronounced in acidic environments compared to neutral environments.[97] Taken together, increased temperature and acidic environments can enhance hydrolysis. Generally, MOFs exhibit a lower chemical stability than their metal oxide counterparts due to the covalent binding of MOF metal clusters and organic linkers that makes them more prone to hydrolysis. However, this "Achilles heel" holds the potential to be used in acidic environments as a stimulus for drug release. An example for this is given by Liang *et al.*,[101] where a PBS pH reduction from 7.4 to 6 was sufficient to release an encapsulated macromolecule (bovine serum albumin (BSA)) from a zinc-based ZIF-8 MOF. ZIF-8 MOFs are a widely studied material for drug delivery applications.[106] Iron oxide nanoparticles are also prone to hydrolysis, undergoing degradation to ferrihydrite and losing their magnetic properties.[88]

The pH, however, not only significantly influences hydrolysis, but also drives reduction–oxidation (redox) reactions (Fig. 2B). In redox reactions, electrons are generally transferred between a NM and its chemical environment. The pH plays a pivotal role in this respect as it influences the redox potential and thereby the capability of the NM to acquire or loose electrons. For example, an increased transformation of Au^0 NP into ionic gold, in which Au^+ seems to be more stable in biological environments than Au^{3+} (Fig. 2B), occurred in acidic (pH 2) and neutral (pH 7) saline solutions (NaCl), whereas under basic conditions (pH 12), this reaction was prevented. This shows that pH is a driving force in redox reactions, with the constraint that the associated experiments were performed under a focused electron beam, which might have had its own influence on the transformation.[82,107] Additionally, the oxidation state of the target element can be altered *via* electron transfer, *e.g.*, by the transfer of free electrons or highly reactive

Table 1 Summary of studies investigating nanomaterial transformations along with the respective transformation reactions, important parameters, and analytical techniques

NM	Chemical formula (MOFs only linker)	Environment	Transformation type	Details of reaction mechanism	Kinetics: max. reaction time	Analytical technique(s)
Metals						
AgNP[79]	Ag^0	In vitro, cell culture medium	Corrosion[a] (Ag_2S formation), complexation (Ag-cystein, -histidine, -acetate)	NA	24 h	ICP-MS synchrotron XAS (XANES)
AgNP[80]	Ag^0	In vitro (THP-1)	Oxidation (Ag_2O); Complexation with macromolecules	$Ag^0 \rightarrow Ag^+$ and AgO-R $\rightarrow AgS$-R	48 h	Synchrotron (X-ray microscopy, XANES)
AgNP[81]	Ag^0	In vitro	Complexation (AgO-R, AgS-R); Dissolution (Ag^+); Oxidation (Ag_2O) Complexation (AgO-R, AgS-R)	$Ag^0 \rightarrow Ag^+$ (50% within 1 h) $\rightarrow AgO$-R (after 12 h) $\rightarrow AgS$-R (stable)	24 h	XANES
AuNP[82]	Au	In vitro primary fibroblasts, lysosomes	Redox reaction: dissolution and recrystallization Secondary NP generation (nano leaves)	1st stage: Fenton/$OH^\bullet$[83] (mediated by NADPH oxidase) → release of ionic Au; 2nd stage: recrystallization of ionic Au (ev. mediated by metalthioneines)	6 months	Electron microscopy (HR-TEM, SAED, STEM, EDX)
Metal oxides						
CeO_2, TiO_2[84]	CeO_2, TiO_2	In vivo mice – intra-venous & intra-tracheal administration	Redox reaction: dissolution, generation of secondary NP	Suggested transformation (oxidation) route published by Graham et al.[85]	180 d	(sp)IC-PMS
CeO_2[85]	CeO_2	In vivo rat liver	Redox reaction: dissolution and recrystallization	Redox reaction ($Ce^{IV} \rightarrow Ce^{III}$), partial dissolution of high energy edge sites and recrystallization to generate ultra-small secondary NP (1–3 nm), associated changes in morphology	90 d	Electron microscopy (TEM, SAED, EELS, EDX)
CeO_2[42]	CeO_2	In vivo rat (liver and spleen)	Corrosion: dissolution, recrystallization	Differences in transformation between liver and spleen; liver: similar to Graham 2014,[85] spleen: lesser degree of "bioprocessing", formation of Ce-phosphates	90 d	Electron microscopy (HR-TEM, STEM SAED, EELS, EDX)
CdSe@ZnS[86]	CdSe@ZnS core shell QDs	In vivo mice (balb/c, liver, spleen, lung, blood, kidney, intestine, urine, faeces)	Dissolution (Zn^{2+}); Reaction with phosphorous ($Zn_3(PO_4)_2$); Corrosion: formation of CdS from CdSe; Complexation: Zn-/Cd-/Se-cysteine, Zn-histidine, Zn-citrate, Se-methionine	Organ specific transformation of all elements: Zn from the ZnS shell (e.g., to $Zn_3(PO_4)_2$ and different other species (e.g. Zn-cysteine) in blood and quick (~10 d) transformation to mainly $Zn_3(PO_4)_2$ in liver, spleen and lung), integration of Zn from ZnS to biomolecules similar to Cao et al.[87] Slow transformation of Se from CdSe to endogenous Se forms (mainly selenomethionine, selenocysteine). Slow transformation of Cd from CdSe to Cd-cysteine and CdS	1, 10, 30, 90, 150, 365 d	XANES

Table 1 *(Contd.)*

NM	Chemical formula (MOFs only linker)	Environment	Transformation type	Details of reaction mechanism	Kinetics: max. reaction time	Analytical technique(s)
Hollow CuS NP/iron oxide nanoflower hybrids[70]	Cu$_{2-x}$S, Fe-oxide (maghemite)@CuS	In vitro human mesenchyma cells and Glioblastoma cells U87	Corrosion: dissolution, recrystallization (Fe)	Transformation of maghemite-Fe to ferrihydrite-Fe, possibly stored within the ferritin protein. Although no phase change was observed for sulfide-Cu, the initial CuS particle size and structure was not preserved per TEM imaging	3 d, 21 d	XANES, electron microscopy (TEM)
γ-Fe$_2$O$_3$ (maghemite)[48]	Fe$_2$O$_3$	In vivo mice (lysosomes) – retro-orbital injection, spleen and liver	Chelation: dissolution and amorphization	Transformation to amorphous, non-magnetic Fe in spleen and liver – potentially in lysosomes, formation of ferritin-Fe	44 d	FMR, SQUID, electron microscopy (TEM, SAED, EDX)
γ-Fe$_2$O$_3$ (maghemite)[88]	Fe$_2$O$_3$	In vitro mesenchymal stem cells (endosomes) 2D and 3D	Dissolution-recrystallization	Degradation by stem cells, generation of secondary NP with poorer crystallinity that remagnetized, ferrihydrite generation	NP uptake 30 min, 21 d	Electron microscopy (TEM, SAED)
Fe-oxides (magnetite) with PEG shell coating[44]	Fe$_2$O$_3$	In vivo rats	Dissolution, degradation	Transformation of magnetite-NP to ferritin-iron (Fe-hydroxide/oxide bound to a Ferritin complex), mainly in the liver	24 h, 7 d, 30 d	Electron microscopy (TEM)
Fe-oxides (maghemite), Fe$_2$O$_3$ citrate-coated[89]	Fe$_2$O$_3$	Endosomal fluid pH 4.7 with citrate; In vitro MSC spheroids (3D)	Chelation: dissolution		27 d	TEM; Magnetometry; Magnetometry
Fe$_3$O$_4$ (FDA approv.) (maghemite)citrate and phosphonoacedic coated[90]	Fe$_3$O$_4$	Artificial lysosomal fluid (ALF) containing citrate, pH 2.5, 3.5, 4.5, RT/37 °C	Chelation: dissolution, loss of crystallinity, secondary species generation	Iron ion release, iron citrate complex; Size reduction – coating dependent; Decrease of saturation magnetization	24 h	ICP-OES, PXRD, DLS, TEM
Fe-oxides (maghemite), multi-core nanoflowers[91]	Fe$_2$O$_3$	Artificial lysosomal fluid (ALF) containing citrate, pH 4.7, 37 °C	Chelation and corrosion: dissolution	Fe-chelate formation with citrate, transformation of multi-core into single-core magnetite-NP	1–90 d//23 d	Magnetometry (FMR – ferromagnetic resonance spectroscopy), SAR (specific absorption rate), electron microscopy (HR-TEM, EFTEM, EDX)
InP QDs (core/core–shell)[92]	Core: InP; 1st shell: ZnSe$_x$S$_{1-x}$; 2nd shell: ZnS	Hydra vulgaris (eukariotic)	Ligand exchange	Damage in atomic structure after 30 min, formation of holes in the atomic structure. In–O bonds get replaced by In–P/In–S bonds (1 h after treatment). High affinity of COO$^-$ for In^{3+}. 1. Phase transition (ligand exchange). 2. Degradation in absence of protective shell	1, 3, 24, 48 h/3 h	μXANES, XRF
MoS$_2$ 2D nanodots[87]	MoS$_2$ conjugated to human serum albumin (HSA)	In vivo C57BL/6 mice, in vitro embryonic murine hepatocyte cell line BNL CL.2 and murine monocyte/macrophage cell line J774A.1	Redox reaction	Formation of protein corona, oxidation of Mo(IV) to Mo(VI) in the liver mediated by phase I oxidases, formation of (MoO$_4$)$^{2-}$, Mo from MoS$_2$ used for biosynthesis of Mo-enzymes such as aldehyde oxidase and xanthine oxidoreductase, which are able to generate factors for tumor progression	6 h, 1 d, 3 d, 7 d, 14 d, 60 d	XANES, XPS
Rare earth oxide NPs[93]		E. coli	Corrosion: dissolution	Formation of Gd-phosphates and carboxylates after NP-cell contact	2 h	XAFS
Metal organic frameworks (MOFs)						
A diverse set of MOFs (e.g., Mn-MOF-74)[94]		Cell culture medium 10% FBS, 37 °C	Corrosion: pot. ligand exchange, amorphization	n/a/phase transformation (generation of new rod-like MnCO$_3$ particles)	24 h	PXRD, ICP-OES, electron microscopy (TEM, SAED)

Table 1 *(Contd.)*

NM	Chemical formula (MOFs only linker)	Environment	Transformation type	Details of reaction mechanism	Kinetics: max. reaction time	Analytical technique(s)
Mg-gallate[95]	$C_6H_2(OH)_3COOH$ Gallic acid (H_4gal)	Water, RPMI cell culture medium, 37 °C	Corrosion: ligand exchange	n/a/formation of Mg-phosphate. Complexation with phosphate is suggested Gallic-acid release was faster in P rich medium	24 h	PXRD, $^{13}C/^1H$ NMR, HPLC
MIL-100 (Fe)[96]	$C_6H_3(CO_2H)_3$ Trimesic acid	Simulated body fluids, PBS (different P concentrations), 37 °C	Corrosion: ligand exchange, amorphization	Replacement of trimesate linker by phosphate ions (ligand-exchange) independent of P content, limited by diffusion of phosphate into and linker out of the MOF → formation of amorphous Fe-phosphate shell	1–8 d (microMOFs)	PXRD, Raman microscopy, Mössbauer spectrometry, electron microscopy (TEM)
MIL-100 (Fe), MIL-53 (Fe)[97]	MIL-100: $C_6H_3(CO_2H)_3$ Trimesic acid MIL-53: $C_6H_4(CO_2H)_2$ Terephthalic acid	Water (100 °C) Water (RT, pH 7)	Hydrolysis	Formation of amorphous ferrihydrite from MOF hydrolysis at pH 7: (a) $2[Fe_3O(OH)(H_2O)_2][BTC]_2 + 7H_2O \rightarrow 3\{Fe_2O_3 \cdot 2H_2O\} + 4H_3BTC$ (b) $2Fe(OH)BDC + 3H_2O \rightarrow \{Fe_2O_3 \cdot 2H_2O\} + 2H_2BDC$ BDC = 1,4-benzenedicarboxylate (MIL-53) BTC = 1,3,5-benzenetricarboxylate (MIL-100)	2 h, 24 h	PXRD, electron microscopy (TEM, SEM)
MIL-100 (Fe)[45]	$C_6H_3(CO_2H)_3$ Trimesic acid	*In vivo* wistar rats	Corrosion: dissolution, ligand exchange	BTC/trimesate and Fe release by replacement with phosphates	15 min–1 h after administration	HPLC
MIL-100 (Fe)[98]	MIL-100: $C_6H_3(CO_2H)_3$ Trimesic acid	Water, PBS, PBS + BSA 37 °C HCL pH 1.2, lis-SIF, lis-SIF + pancreatin, lis-SIF + mucine 37 °C	Hydrolysis: ligand exchange, degradation	Linker (BTC/trimesate) release into medium	Up to 24 h	HPLC, XRPD
MIL-88A (Fe), MIL-100 (Fe)[46]	MIL-88A: $HO_2CCH=CHCO_2H$ Fumaric acid MIL-100: $C_6H_3(CO_2H)_3$ Trimesic acid	Simulated physiological conditions *In vitro* mouse macrophages *In vivo* wistar rats	Ligand exchange, amorphization	Linker release and degradation of nano MOF	*In vitro* 8 d *In vivo* 3 months	HPLC, SEM
PCN-223 (Zr)[99]	$C_9H_{18}Cl_3O_4P$ Tris-(2-chlorisopropyl)-phosphat	Water, PBS, cell culture medium	Degradation		Up to 7 d	
UiO-66/UiO-66-PEG (Zr)[100]	C_6F_4-1,4-(CO_2H) 1,4-Benzenedicarboxylic acid	PBS	Ligand release/exchange, degradation, amorphization	Linker release speed dependent on surface modification and pH	Up to 24 h	UV-Vis, PXRD
ZIF-8 (Zn), Comparison micro- and nano-sized[78]	$C_4H_6N_2$ 2-Methylimidazol	PBS pH 7.4, 37 °C	Corrosion: ligand exchange	Competition of phosphate for metallic centers, linker release, conversion of rhombic dodecahedron ZIF-8(Zn) to spherical Zn-phosphate NP	Main changes in 1st hour//1, 3, 6, 24 h	PXRD, IR, electron microscopy (SEM, EDX), AFM, GC-MS
ZIF-8 (Zn)[101]	$C_4H_6N_2$ 2-Methylimidazol	Solution with biomacromolecules (proteins, DNA, enzymes)	Hydrolysis: decomposition	Change in acidity from pH 7.4 to 6 37 °C disintegrates ZIF-8 layer		PXRD, electron microscopy (SEM)

[a] Definition of corrosion in terms of chemistry according to Ahmad 2006:[102] "Corrosion is the gradual destruction" or "Corrosion is the destructive attack of a metal and environments which results in its destructive attack of a metal by chemical or electrochemical reaction with the environment" (examples are rust formation, sulfidation of metallic Ag *etc.*). For example, the reaction of Fe^{2+} with water under oxygenated conditions to give $2Fe_2O_3 \cdot xH_2O$.
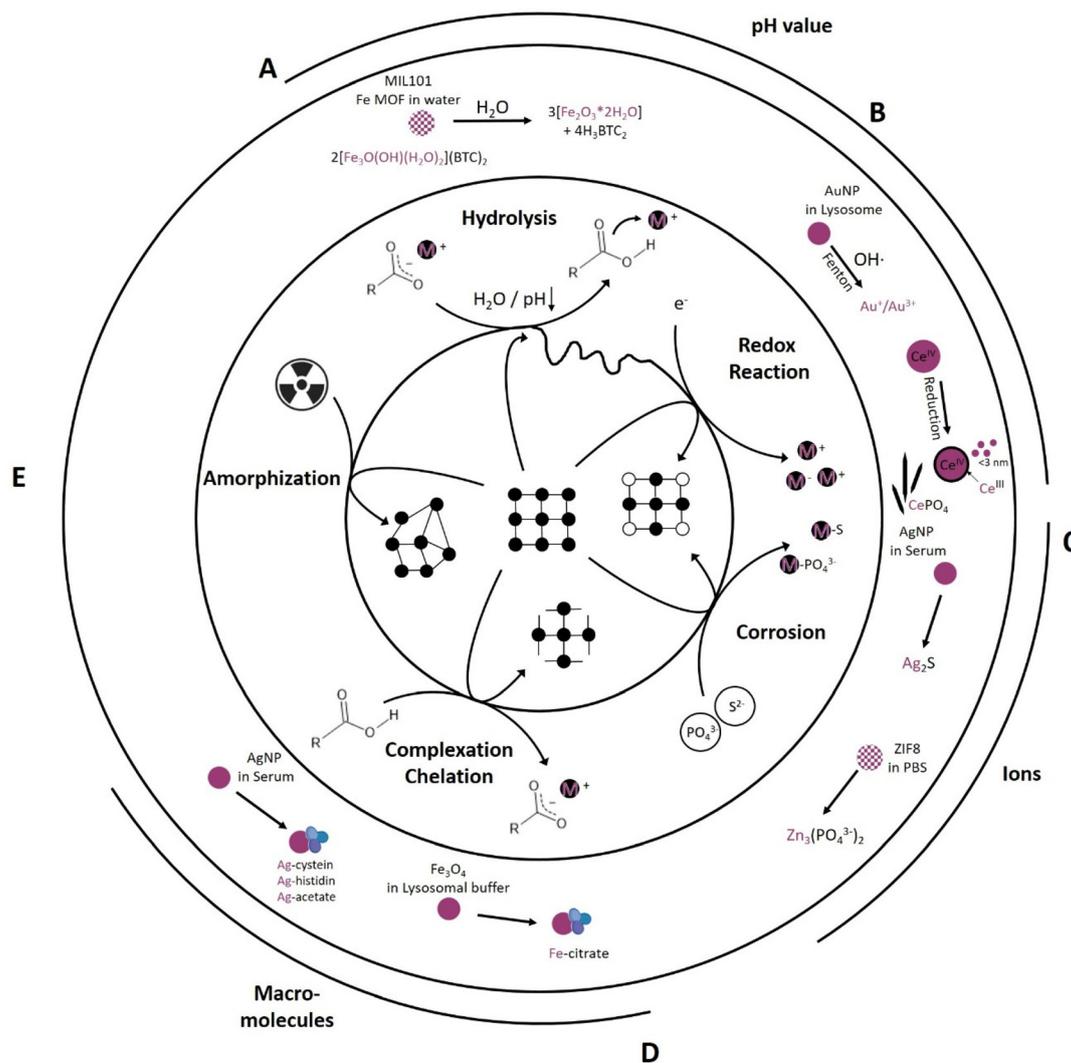
Fig. 2 Primary reactions initiate transformation of inorganic NM dependent on the chemical environment including (A) hydrolysis reactions (*e.g.*, MIL-101 transformation into an amorphous ferrihydrite[97]), (B) redox reactions (*e.g.*, AuNP transformation into Au$^+$/Au^{3+} (ref. 82) and formation of Ce^{III} surface sites on CeO$_2$ as well as formation of Ce-phosphate needles *in vivo*[42,43]), (C) corrosion reaction (*e.g.*, AgNP transformation into Ag$_2$S[79] and ZIF-8 transformation into Zinc phosphate[78]), (D) complexation and chelation reactions (*e.g.*, Fe$_3$O$_4$ transformation into Fe-citrate[90] and AgNP transformation into Ag-cystein/-histidin/-acetate[79]), and (E) radiation induced amorphization reaction.

radicals, such as reactive oxygen species (ROS). In physiological environments, in addition to purely chemically driven redox reactions including Fenton-like[108] reactions also enzyme-mediated reactions can occur. Enzymes, such as superoxide dismutase (SOD) or catalase (CAT), maintain the redox balance in physiological environments to support cellular health and functionality. SOD catalyzes oxidation reactions, converting highly reactive oxygen (superoxide, O^{2-}) to hydrogen peroxide (H$_2$O$_2$) and oxygen (O$_2$), whereas CAT catalyzes reduction reactions, in which the H$_2$O$_2$ is further converted to water and oxygen. Therefore, CAT and SOD play pivotal roles in cellular oxidative stress protection.[109–112] An example of enzyme-mediated oxidation is one involving 4 nm gold nanoparticles (Au^0 NPs), which are generally believed to be chemically inert. Balfourier *et al.* proposed a complex biotransform-

ation reaction, where in a first stage the NOX complex (membrane associated protein complex: NADPH oxidase) converted O$_2$ into ˙O$_2^-$, followed by its conversion into H$_2$O$_2$ *via* SOD. Hydrogen peroxide then oxidized the Au^0 NP into ionic gold *via* a Fenton reaction, resulting in either Au$^+$ or Au^{3+} (Fig. 2B).[82] Besides SOD mediated H$_2$O$_2$ generation also a spontaneous dismutation is conceivable, most likely due to the reduction of O$_2$ to ˙O$_2^-$ in the mitochondrial respiration pathway.[113] Therefore, depending on the source of the ROS, the transformation is either a bio- or chemical transformation. Another example of a redox reaction is the *in vivo* reduction of Ce^{IV}O$_2$ particles. As-synthesized 30 nm cubic Ce^{IV}O$_2$ particles were analyzed 90 days after IV injection in rat liver and spleen. *In vivo* dissolution of high energy edges occurred, resulting in a rounded morphology with increased Ce^{III} levels in the shell

region. The transformation rate in the liver, which possessed a higher acidity, was higher than that of the spleen. These findings were consistent with previous work that showed that the transformation rate of ceria was dependent on pH and electrochemical potential. The *in vivo* dissolution of these $Ce^{IV}O_2$ particles resulted in the formation of Ce^{III} enriched clouds as well as the recrystallization of ultra-small 1–3 nm CeO_{2-x} particles; these particles had a significantly increased free radical scavenging potential (antioxidant effect) (Fig. 2B).[43,114] Following the Ce^{III} ion release, Graham *et al.* observed tissue-dependent phosphatization and recrystallization in form of $Ce^{III}PO_4$ nanoneedles, with an individual length of about 20 nm being part of a greater network.[42] Generally, metals, such as cerium, iron, chromium and nickel are known to catalyze Fenton-like reactions *in vitro* and *in vivo*.[108,115,116] Also, some metals or trace elements are essential for the body and were recently shown to be converted to active biological molecules, thus over time exerting an effect on the metabolism.[86,87] For example, Mo was shown to be integrated into Mo-cofactors in the liver after enzyme-mediated oxidation of Mo(IV) to Mo(VI) from MoS_2 particles. This in turn led to an increased activity of the main molybdoflavoenzymes (aldehyde oxidase and xanthine oxidoreductase) which can generate nitric oxide, involved in tumor progression.[87] Thus, metals should be closely monitored over their entire *in vitro* or *in vivo* life cycle if considered for biomedical applications to ensure their efficacy and safety.

Like hydrogen and oxygen, sulfur and phosphorous are essential and abundant elements in physiological environments. Sulfur is present in different forms, such as sulfate (SO_4^{2-}), sulfides (S^{2-}), and thiol groups (–SH), in proteins and cellular structures. Phosphorous is an integral component of biological molecules, nucleic acids (DNA and RNA), adenosine triphosphate (ATP), and phospholipids, the building blocks of the cell and cell organelle membranes. In their different forms, depending on the composition and affinity, those ions can interact with NMs. Here, we term the underlying chemical reaction "corrosion", which leads to the gradual destruction of an NM as the ion reacts with the metal, resulting in the formation of metal-sulfides or metal-phosphates in amorphous or crystalline forms (Fig. 2C). The metal-sulfide or metal-phosphate can also still be bound to the macromolecule and therefore forming metal-sulfide- or metal-phosphate-complexes.[80] The corrosion of the chalcophile silver (Ag) (-NP) with *e.g.* H_2S into Ag_2S is widely known and has been described for different systems were sulfur-bearing species are prevalent, significantly impacting behavior and fate of the material in the different systems.[117–120] In biomedical applications, silver nanoparticles (AgNPs) are studied for their antimicrobial properties,[121] advanced wound healing properties,[122,123] implant coating properties,[124] and applicability in drug delivery systems.[125] In *in vitro* lymphocyte experiments, Ag either stayed intact as metallic silver or was transformed into Ag_2S in a corrosion reaction or complexed as Ag-cystein.[79] The transformation and fractionation into intact AgNPs, Ag_2S, and Ag-cystein was highly dependent on the original particle size. The smaller the

as-synthesized particle, the higher the uptake and intracellular sulfidation into Ag_2S in contrast to a lower AgNP uptake and intracellular sulfidation for bigger as-synthesized particles (Fig. 2C).[79] Jiang *et al.* and Wang *et al.* proposed a multiple-step intracellular transformation that saw the dissolution of Ag^0 NP to Ag^+, followed by an oxidation to Ag–O species after 12 h and a sulfidation to Ag_2S after 24 h, resulting in a more stable intracellular form compared to the intermediate states.[80,81] Also, the phosphatization of zinc-based ZIF-8 MOFs has been found to exhibit particle-size-dependent transformation kinetics. Phosphates in PBS were found to compete with the linker of the framework structures, resulting in a release of the linker and a conversion of the rhombic, dodecahedron ZIF-8 particles into spherical, amorphous Zinc phosphate particles (Fig. 2C).[78] This process was highly particle-size-dependent, with a faster transformation for smaller nano-sized ZIF-8 particles.[78] Similarly, also Zn from ZnS shells was shown to transform (amongst others) into $Zn_3(PO_4)_2$.[86] Also other elements with a high affinity towards specific S- or P-bearing species are likely to be subject to corrosion (*e.g.* Cu^{126} or Cd^{86}). This transformation will alter biocompatibility and nanomedical application efficiency. A better understanding of the underlying corrosion mechanisms can help to improve stability and reduce undesired side effects, already during the NM design and synthesis. The synthesis could be augmented by *e.g.*, mesoporous silica shells[127] or organic polymer coatings, such as poly ethylene glycol (PEG)[128] coatings, to protect the material from corrosion. For semi-conductor NM, ZnS is sometimes proposed as a protective shell. However, recently, Chen *et al.* showed that a ZnS shell can be rapidly degraded within 10 days in an *in vivo* setting.[86] Ultimately, whether a more protective or a more labile shell is required will depend largely on the needs of the final application and/or on the clearance pathways of the respective NM and its constituent elements.

So far, only interactions between ions and small molecules have been discussed. However, physiological environments also contain larger and complex (macro) molecules, such as proteins, amino acids, and other organic molecules. These molecules have key functional moieties, such as carboxyl- (–COOH), amino- (–NH2), aldehyde- (–C(=O)H), and thiol (–SH) moieties, which can interact and coordinate NM-related elements/ions. Generally, metal coordination, complexation, and chelation processes (Fig. 2D) play a key role in cellular metabolism and signaling, *e.g.*, in metalloenzymes such as peptidases, the zinc finger-proteins of transcription factors, oxygen transport *via* hemoglobin and excretion. As chelation and complexation are systemically present, and many protein functional groups can function as chelators, they influence NM cellular fate. AgNPs have been shown to transform apart from the main product Ag_2S also into Ag-cysteine, Ag-histidine, and Ag-acetate complexes (Fig. 2D).[79] The proportional distribution of Ag-cysteine, Ag-histidine, and Ag-acetate complexation was surface-functionalization and particle-size dependent; for example, no Ag-cysteine complexes were found for differently sized citrate-capped AgNP, whereas the opposite was the case for polyethylenimine-(PEI)-coated AgNPs.[79] Gutiérrez

et al. also proved the impact of surface functionalization on chelation kinetics.[90] This study used citric acid (CIT) and phosphonoacetic acid (PAA) on magnetic Fe-oxides (Fe_3O_4) in 20 mM citric acid lysosomal mimicking buffer (pH 2.5, 3.5, and 4.5).[90] The transformation was faster for PAA-functionalized particles than for CIT-functionalized particles, with a size reduction and faster transformation in strong acidic environments (pH 2.5). They compared the temperature (RT and 37 °C) dependence at pH 4.5 and found a tremendous impact on transformation kinetics for both coatings, with a significantly faster transformation for PAA-functionalized Fe-oxides (Fig. 2D).[90] Surface functionalization and coatings potentially protect NMs from chelation and complexation; *i.e.*, the metal centers are shielded from the chelators and complexing agents by the coating layer. Therefore, a denser and thicker coating might improve the protection, but at the same time hamper applications relying on core material activity.

So far, all primary transformation reactions discussed were induced by the chemical environment, *i.e.*, the concentration and combination of ions, the pH (basic, neutral, acidic conditions), or presence of macromolecules and proteins. However, external factors, such as radiation, are known to induce transformation (Fig. 2E). To our knowledge this has not yet been studied for biomedically relevant nanomaterials. Except for Lin *et al.*, who has introduced the first radio-enhancing Hf-based MOF, RiMO-301, which is currently under clinical trials (Phase I: NCT03444714). They did not find any phase transformation upon 16 Gy X-ray (250 kVp, 15 mA, 1 mm Cu filter) irradiation.[129] However, since radio-enhancement applications of nanomaterials have found increasing potential, phase transformation must be carefully considered if ionizing radiation is applied.

In other fields, radiation-induced transformations have been observed; for example in waste management, hydroxyapatite nanoparticles ($Ca_{10}(PO_4)_6(OH)_2$) are used for the disposal of actinides and fission products.[130] These particles amorphize under 1 MeV Kr^{2+} ions in a size-dependent manner (20 to 280 nm); the smaller the particles, the faster the amorphization process. This suggests a surface-to-volume enhanced transformation process due to the fast accumulation of oxygen vacancies. Interestingly, after amorphization, they observed a transmission electron microscope-induced (electron energy of 200 keV) recrystallization, again size dependent, with a significantly faster recrystallization process into smaller hydroxyapatite nanoparticles, respective to the native particle size.[130] Furthermore, influence of particle size on radiation-induced amorphization has been studied. Smaller $CePO_4$ particles (20 nm) underwent faster amorphization at RT, than larger particles (40 nm) under 1 MeV Kr^{2+} irradiation. It was proposed that for smaller NP a proportionally higher fraction of amorphization induced swelling and deformation which led to a faster complete loss of crystallinity. This effect was further increased for both particle sizes in higher temperature conditions (100 °C).[131] However, there are also the opposite indications, that small single crystals/grains can enhance radiation tolerance, *i.e.* the resistance to phase transitions.[132,133] The

mechanisms governing this dependence remain yet to be determined.

Harnessing analytics to unravel (bio-) transformation processes

Generally, the analysis of (bio-)transformations of inorganic nanomaterials in a near native manner and based only on minimal perturbation of the system is key. However, high-resolution chemical and structural analysis relies on adequate sample preparation and analysis settings. These often necessitate analysis under vacuum conditions and might involve other modifications to the system, such as introducing labels. In particular, the introduction of widely used (fluorescence)-labels, *e.g.*, for the visualization of metal ions or entire nanoparticles has a high potential for critical alteration of the system. Similarly, also the use of high-vacuum analytical techniques, such as (analytical) electron microscopy or X-ray photoelectron spectroscopy, which require sample drying, and sometimes even chemical fixation, heavy metal staining and/or embedding into resin can bear considerable source for sample preparation artifacts. In addition, also measurement induced changes need to be carefully considered, including damage induced by the electron beam of the electron microscope (*e.g.* through knock-on displacement, radiolysis or electrostatic charging and heating), potential re-crystallization of amorphous materials under the electron beam or changes induced by sample heating when using lasers, *e.g.* in vibrational spectroscopy. However, many challenges, such as sampling artifacts, sample heating, and other beam-induced damages, can be mitigated by using cryogenic conditions (typically characterized as temperatures below −150 °C (ref. 134)). By employing these methods along with other meticulous sampling strategies that prevent further reactions of the analytes, "snapshots" of the processes can be obtained.

Hence, all analytical investigations need to be carefully designed to include appropriate controls that help to identify potential errors. Also, the use of as many as possible complementary and/or orthogonal techniques[135] is highly advisable in order to reduce uncertainty and increase consistency of the data and hence their trustworthiness. This becomes even more important, as in some cases observing no change in one parameter does not mean that there is no change also in another – as shown for CuS particles that showed no phase change in X-ray absorption spectroscopy but significant morphological changes in electron microscopy.[70]

In the following, analytical techniques suitable to give insights into the respective previously discussed reaction mechanisms (Fig. 3) will be systematically discussed.

Changes to the material that involve structural changes together with release of components (*e.g.* hydrolysis, dissolution in general) require a combined approach including electron microscopy and elemental analysis, eventually together with chromatographic techniques (Fig. 3A and B). For example, imaging techniques such as high-resolution (scan-
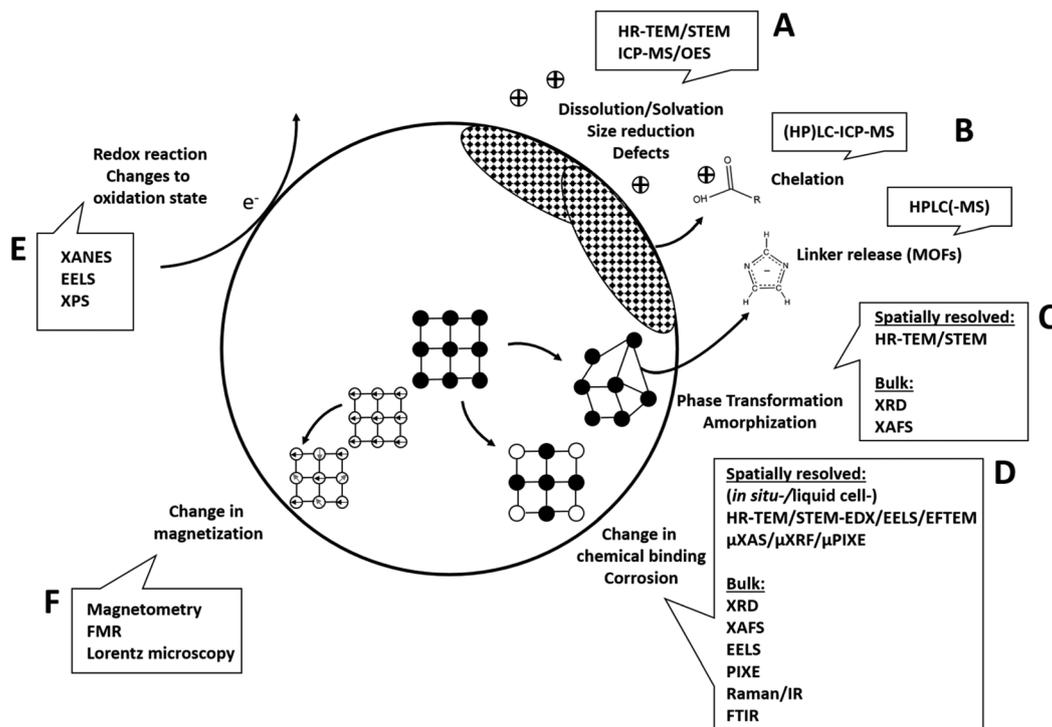
Fig. 3 Analytical techniques to unravel underlying transformation processes. (A) Structural changes and accompanying ion release can be analyzed using a combination of high-resolution (scanning) transmission electron microscopy (HR-TEM/STEM) and inductively coupled plasma mass spectroscopy or optical emission spectroscopy (ICP-MS/OES). (B) Organic components (*e.g.* MOF linkers, surface molecules) released from the solid material can be analyzed with high performance liquid chromatography (HPLC). (C) Phase transformations including amorphization can be analyzed with HR-TEM/STEM, bulk X-ray diffraction (XRD) or X-ray absorption fine structure/extended fine structure spectroscopy (XANES/EXAFS). (D) Corrosion, complexation and changes in chemical binding can either be analyzed with high spatial resolution using HR-TEM/STEM combined with energy-dispersive X-ray spectroscopy (EDX) or electron energy loss spectroscopy (EELS, EFTEM) as well as X-ray micro/bulk-analysis, *e.g.*, (micro-)X-ray absorption spectroscopy (XANES/EXAFS, μXAS), micro-X-ray fluorescence (μXRF), micro-particle induced X-ray emission (μPIXE). (E) For analysis of changes in oxidation state EELS, X-ray absorption near edge spectroscopy (XANES) or X-ray photoelectron spectroscopy (XPS) are the techniques of choice. (F) Magnetic materials as well as changes in magnetic potential is analyzed using magnetometry, ferromagnetic resonance (FMR) or Lorentz microscopy.

ning) transmission electron microscopy (HR-(S)TEM) in combination with EDXS can be employed to study structural and compositional changes to the solid phase (dry or cryogenically preserved), while the fractionation between solid and dissolved components can be studied using inductively coupled plasma techniques (ICP-OES or -MS, liquid samples (aqueous or organic)) together with suitable separation techniques (*e.g.* filtration, centrifugation). In addition, single particle ICP-MS gives access to particle size distribution (see *e.g.* Modrzynska *et al.*[41]). Here, transient signals of highly diluted particle dispersions are being recorded, where single particle events can be distinguished from a dissolved background. The intensity distribution of these events can then be converted to a particle size distribution, where the specific geometry has to be known or assumed. Detection limits in terms of particles size mostly depend on the constituent element and have been evaluated.[136] Size detection limits are lowest for the more heavy elements, for example therapeutically relevant Hf or Ce-oxides can be determined down to ≈10 nm, whereas most of the other relevant elements such as Zn or Fe are detectable roughly down to 30–50 nm or even >100 nm (Si, Ca).

Conventional quadrupole ICP-MS systems are only able to measure one element at a time, so for materials where multiple elements have to be monitored, a more costly time-of-flight (TOF) analyzer has to be used. Such an analyzer is capable of simultaneous detection across almost the entire mass range between 7 and 275 amu.[137] This additionally gives access to monitoring compositional changes to the individual NPs (*e.g.*, making use of isotope labelling), which makes this technique very powerful for biotransformation studies.[138]

For organo-metallic materials, such as MOFs, it is necessary to additionally monitor the release of organic building blocks and/or metabolites. In the absence of interfering absorbers, this can be achieved using rather straightforward techniques such as UV-Vis spectroscopy[100] or, if more detail and higher sensitivity is required, more advanced techniques such as high performance liquid chromatography (HPLC) with coupling to UV detection[46] and/or mass spectrometry (MS, Fig. 3B, transfer of the analytes to compatible solvents might be necessary). However, some biogenic organic molecules can also act as chelating agents, able to complex metals and act as promotors of dissolution within the cell/body. To study chelation processes

or generally binding of organic molecules to inorganic ions, a combination of HPLC and ICP-MS is usually employed.[139] For inorganic complexes, ion chromatography in combination with ICP-OES/MS is a potent technique combination.

Changes in bulk phase and crystallinity are commonly assessed using X-ray diffraction (XRD, see *e.g.* ref. 78). However, this often requires the availability of larger sample amounts in the order of mg to g,[140] depending on the sample (usually dry powders). While these amounts are mostly available for the initial materials, this is not the case after experiments conducted with relevant dosing. Also, XRD shows significant peak broadening with decreasing particle size, making the characterization of very small (<10 nm) particles challenging.[141] Here, complementary to bulk XRD, high resolution (HR) – (scanning) transmission electron microscopy ((S)TEM) in combination with electron diffraction can be used on single particles to determine their crystal structure, requiring only minor sample amounts. Furthermore, due to the size-related peak broadening in XRD, the comparison of (S)TEM-determined particle size to XRD-determined particle size can allow conclusions regarding the dominating size fraction in the sample.[141] In addition, most microscopes capable of analyzing electron diffraction are equipped with an energy dispersive X-ray spectrometer (EDXS), which allows to determine the elemental composition of the particle. This classic combination of XRD and electron microscopy has been used with success in many of the reviewed studies. For example, Graham *et al.*[42] used a combination of electron diffraction and EDX elemental mapping to follow the transformation of nano-ceria in an *in vivo* setting.

However, new developments in terms of automation in electron microscopy might revolutionize the way in which this set of techniques can be applied to study particles even in complex environments such as cells. For example, pieces of software are already available that allow a fully automated analysis workflow consisting of image acquisition, particle identification, particle compositional analysis using EDX and particle size and morphological characterization.[142] Also, more and more free software is available that aids image based particle analysis (see for example the Particle-Sizer plugin for ImageJ[143]). Such automated routines give access to much better statistics, as thousands of particles can be analyzed in a rather short time. As the development of artificial intelligence is progressing rapidly, our capabilities of automatically recognizing and analyzing particles in complex environments will increase drastically in the future (see *e.g.* ref. 144), potentially making electron microscopy a key technique for biotransformation studies. Also in terms of changes to the oxidation state of atoms, electron microscopy plays an important role, as this parameter is accessible from electron energy loss spectroscopy (EELS, Fig. 3E) in specialized TEMs. With EELS, the electronic structure and chemical bonding can be analyzed at the nanoscale as the energy distribution of the electrons is analyzed after their interaction with the sample. The combination of STEM and EELS allows for a very detailed characterization of complex NMs, apart from element identification and oxidation state also yielding valuable information such as element molar ratios or identification of specific carbon bonds of organic coatings.[145] Apart from analysis of single particles/pure materials, EELS can also be applied to (embedded) cells/tissues.[146] Here, EELS can especially serve to collect complementary biological information, such as mapping the distribution of proteins or water in the cell by low-energy loss EELS. Also, studies are available that analyzed NM transformation in tissues using EELS, *e.g.* CeO_2 in the liver of rats.[85] Here, the high spatial resolution of STEM-EELS allowed to discriminate between Ce^{III} on the surface of single particles as opposed to Ce^{IV} in their center. However, generally, for successful EELS measurements, sample quality is absolutely critical. This includes the absence of carbon contamination build-up, appropriate sample thickness and analyte mass fraction. Measurement temperatures $\leq LN_2$ as well as low-dose techniques are helpful in this regard.

Apart from EELS and X-ray spectroscopy in the EM, X-ray based spectroscopy in general holds a multitude of possibilities for elemental analysis as well as for determination of chemical states and structure. One of the most powerful techniques in this regard is synchrotron X-ray absorption spectroscopy (X-ray absorption near-edge (XANES) and extended X-ray absorption fine structure (EXAFS) spectroscopy), giving access to element oxidation state and local coordination geometry. It can be performed $<LN_2$ temperatures, which allows to resolve material changes in frozen time series with minimal sample alteration. Samples for investigation include cell free systems but can be extended to cells, cell cultures and tissues.[86,147,148] Some beamlines additionally offer the possibility of a micro-focused or even nano-focused (≈ 100 nm^2)[149,150] X-ray beam, adding spatial resolution and resulting in hyperspectral data-cubes.[151] However, either high intracellular analyte element concentrations or high local concentrations of it within the cell are necessary to record interpretable data.[149] In addition, especially with micro/nano-focused beams, potential influences of the X-ray beam on the sample during the measurement have to be taken into account. For cells and/or tissues, sample preparation methods have been mostly adapted from electron microscopy, including classical embedding and sectioning or fully cryogenic preparation.[150]

As a more available, lab-scale technique, X-ray photoelectron spectroscopy (XPS) also allows to access oxidation and binding states as well as general elemental composition (all elements except H and He[152]). Here, mono-energetic soft X-rays are being used to extract electrons from the surface in ultrahigh-vacuum *via* the photo-electric effect, whose energies are subsequently analyzed. This then gives access to the electron binding energies, which inform about the elements chemical state. However, as photoelectrons generally can only escape from a depth roughly below 10 nm, XPS is only sensitive to the sample surface.[152] This makes the technique ideal to study changes to surface terminations and/or coatings. For example, after incubation with glutathione – an important peptide in the body – a reduction of disulfide bonds to thiol groups in the outer layer of organo-silica NPs was observed using XPS.[153] When determining oxidation states however, care has to be taken to account for potential reduction by the

X-ray beam. If reduction is observed, determination of the reduction rate law can still allow to determine the true sample composition by extrapolation to zero X-ray exposure time.[154] To address questions regarding the relevance of XPS to hydrated biological environments, freeze hydration or cryo-XPS was developed almost 30 years ago.[152,155] Here, the sample is fast-frozen in the XPS entry chamber, where the subsequent exposure to ultrahigh-vacuum sublimates the ice. However, it is estimated that during the following XPS analysis conducted below −120 °C about 2–3 layers of water molecules still remain at the surface together with structural water inside the cells.[156] Conducting the analysis at or below cryogenic temperatures then also has been shown to reduce thermal induced beam damage, similar to electron microscopy or other X-ray based techniques.[156]

Finally, changes to magnetic properties can be accessed using magnetometry approaches, including electron paramagnetic spectroscopy (EPR), ferromagnetic resonance spectroscopy (FMR), vibrating sample magnetometry (VSM), Alternating Gradient Field Magnetometer (AGFM)[157] and Superconducting Quantum Interference Device (SQUID)[158] measurements. Also magnetic resonance imaging (MRI), and especially quantitative parameters R_2, R_2^* and QSM have been shown to be sensitive to changes in iron oxidation state.[159]

Conclusions and outlook

A solid understanding of NM (bio-)transformations and their mechanisms opens up entirely new avenues of research. Especially, it increases our ability to predict and explore crucial safety aspects of these materials, which will in turn pave the way for the safe-by-design development of new nanomedicines. Furthermore, (bio-) transformation may be harnessed for diagnostic and therapeutic purposes, giving access to multistage diagnostics or therapeutics. Such materials would undergo chemical changes over time and exert multiple functions. For example, they could provide feedback after initiation of the transformation reaction that could be read out externally, *e.g.*, through changes in medical image contrast. Such feedback could include information either on the tissue environment faced by the nanotherapeutic, or on the status of the treatment (*e.g.*, change in contrast indicating the release of a therapeutic agent). To fully harness these potentials, the community needs to adapt a rigorous testing process that involves *in vivo* experiments complemented by experiments at carefully reduced complexity to unravel underlying mechanisms, all accompanied by multi-scale and multi-modal complementary analytics to fully describe the fate of the materials in the body.

Author contributions

AN: investigation, data curation, writing – original draft; IKH: funding acquisition, resources, conceptualization, writing –

review and editing; AG: conceptualization, data curation, investigation, supervision, writing – review and editing. All authors agreed to the final version of the manuscript.

Conflicts of interest

The authors declare no conflict of interest.

Acknowledgements

References

1 B. Buesser and S. E. Pratsinis, *Annu. Rev. Chem. Biomol. Eng.*, 2012, **3**, 103–127.
2 L. Yang, W. Li, M. Kirberger, W. Liao and J. Ren, *Biomater. Sci.*, 2016, **4**, 785–802.
3 Q. Tang, Z. Zhou and Z. Chen, *Nanoscale*, 2013, **5**, 4541.
4 L. Jing, W. Zhou, G. Tian and H. Fu, *Chem. Soc. Rev.*, 2013, **42**, 9509.
5 P. Mukhopadhyay, R. Mishra, D. Rana and P. P. Kundu, *Prog. Polym. Sci.*, 2012, **37**, 1457–1475.
6 P. Sanderson, J. M. Delgado-Saborit and R. M. Harrison, *Atmos. Environ.*, 2014, **94**, 353–365.
7 S. Anu Mary Ealia and M. P. Saravanakumar, *IOP Conf. Ser.: Mater. Sci. Eng.*, 2017, **263**, 032019.
8 K. Zarschler, L. Rocks, N. Licciardello, L. Boselli, E. Polo, K. P. Garcia, L. De Cola, H. Stephan and K. A. Dawson, *Nanomedicine*, 2016, **12**, 1663–1701.
9 J. Xie, S. Lee and X. Chen, *Adv. Drug Delivery Rev.*, 2010, **62**, 1064–1079.
10 D. Anderson, T. Anderson and F. Fahmi, *Phys. Status Solidi A*, 2019, **216**, 1801008.
11 S. Caspani, R. Magalhães, J. P. Araújo and C. T. Sousa, *Materials*, 2020, **13**, 2586.
12 Z. R. Stephen, F. M. Kievit and M. Zhang, *Mater. Today*, 2011, **14**, 330–338.
13 C. Sun, J. S. H. Lee and M. Zhang, *Adv. Drug Delivery Rev.*, 2008, **60**, 1252–1265.
14 W.-H. Chen, W.-C. Liao, Y. S. Sohn, M. Fadeev, A. Cecconello, R. Nechushtai and I. Willner, *Adv. Funct. Mater.*, 2018, **28**, 1705137.
15 R. Singh and J. W. Lillard, *Exp. Mol. Pathol.*, 2009, **86**, 215–223.
16 A. Guerreiro, N. Chatterton, E. M. Crabb and J. P. Golding, *Cancer Nanotechnol.*, 2019, **10**, 10.
17 K. T. Butterworth, S. J. McMahon, F. J. Currell and K. M. Prise, *Nanoscale*, 2012, **4**, 4830.
18 A. L. Neuer, A. Jessernig, L. R. H. Gerken, A. Gogos, F. H. L. Starsich, A. H. C. Anthis and I. K. Herrmann, *Biomater. Sci.*, 2022, **10**(22), 6558–6569.

19 Z. Kuncic and S. Lacombe, *Phys. Med. Biol.*, 2018, **63**, 02TR01.

20 S. Kumar Nethi, S. Das, C. Ranjan Patra and S. Mukherjee, *Biomater. Sci.*, 2019, **7**, 2652–2674.

21 M. M. Mihai, M. B. Dima, B. Dima and A. M. Holban, *Materials*, 2019, **12**, 2176.

22 A. Barroso, H. Mestre, A. Ascenso, S. Simões and C. Reis, *Nano Sel.*, 2020, **1**, 443–460.

23 H. Zhao, C. Serre, E. Dumas and N. Steunou, in *Metal-Organic Frameworks for Biomedical Applications*, ed. M. Mozafari, Woodhead Publishing, 2020, pp. 397–423.

24 H. Huang, W. Feng, Y. Chen and J. Shi, *Nano Today*, 2020, **35**, 100972.

25 J. M. Metselaar and T. Lammers, *Drug Delivery Transl. Res.*, 2020, **10**, 721–725.

26 L. van der Koog, T. B. Gandek and A. Nagelkerke, *Adv. Healthcare Mater.*, 2022, **11**, 2100639.

27 P. Liu, G. Chen and J. Zhang, *Molecules*, 2022, **27**, 1372.

28 H. Bouwmeester, I. Lynch, H. J. P. Marvin, K. A. Dawson, M. Berges, D. Braguer, H. J. Byrne, A. Casey, G. Chambers, M. J. D. Clift, G. Elia, T. F. Fernandes, L. B. Fjellsbø, P. Hatto, L. Juillerat, C. Klein, W. G. Kreyling, C. Nickel, M. Riediker and V. Stone, *Nanotoxicology*, 2011, **5**, 1–11.

29 T. L. Moore, L. Rodriguez-Lorenzo, V. Hirsch, S. Balog, D. Urban, C. Jud, B. Rothen-Rutishauser, M. Lattuada and A. Petri-Fink, *Chem. Soc. Rev.*, 2015, **44**, 6287–6305.

30 M. Hadjidemetriou and K. Kostarelos, *Nat. Nanotechnol.*, 2017, **12**, 288–290.

31 M. P. Monopoli, C. Åberg, A. Salvati and K. A. Dawson, *Nat. Nanotechnol.*, 2012, **7**, 779–786.

32 G. V. Lowry, K. B. Gregory, S. C. Apte and J. R. Lead, *Environ. Sci. Technol.*, 2012, **46**, 6893–6899.

33 G. Pulido-Reyes, F. Leganes, F. Fernández-Piñas and R. Rosal, *Environ. Toxicol. Chem.*, 2017, **36**, 3181–3193.

34 J. Lv, P. Christie and S. Zhang, *Environ. Sci. Nano*, 2019, **6**, 41–59.

35 M. Ganesh and J. Ramakrishna, *Asian J. Org. Chem.*, 2020, **9**, 1341–1376.

36 M. Fayette and R. D. Robinson, *J. Mater. Chem. A*, 2014, **2**, 5965–5978.

37 Y. Xu, K. Ren, T. Ren, M. Wang, S. Yu, Z. Wang, X. Li, L. Wang and H. Wang, *J. Mater. Chem. A*, 2020, **8**, 19873–19878.

38 C. Zhang, W. Liu, C. Chen, P. Ni, B. Wang, Y. Jiang and Y. Lu, *Nanoscale*, 2022, **14**, 2915–2942.

39 H. Zhou, J. Ge, Q. Miao, R. Zhu, L. Wen, J. Zeng and M. Gao, *Bioconjugate Chem.*, 2020, **31**, 315–331.

40 D. A. Porter and K. E. Easterling, *Phase Transformations in Metals and Alloys (Revised Reprint)*, CRC Press, 2009.

41 J. Modrzynska, T. Berthing, G. Ravn-Haren, K. Kling, A. Mortensen, R. R. Rasmussen, E. H. Larsen, A. T. Saber, U. Vogel and K. Loeschner, *PLoS One*, 2018, **13**, e0202477.

42 U. M. Graham, R. A. Yokel, A. K. Dozier, L. Drummy, K. Mahalingam, M. T. Tseng, E. Birch and J. Fernback, *Toxicol. Pathol.*, 2018, **46**, 47–61.

43 U. M. Graham, M. T. Tseng, J. B. Jasinski, R. A. Yokel, J. M. Unrine, B. H. Davis, A. K. Dozier, S. S. Hardas, R. Sultana, E. A. Grulke and D. A. Butterfield, *ChemPlusChem*, 2014, **79**, 1083–1088.

44 A. Ruiz, L. Gutiérrez, P. R. Cáceres-Vélez, D. Santos, S. B. Chaves, M. L. Fascineli, M. P. Garcia, R. B. Azevedo and M. P. Morales, *Nanoscale*, 2015, **7**, 16321–16329.

45 T. Simon-Yarza, T. Baati, F. Neffati, L. Njim, P. Couvreur, C. Serre, R. Gref, M. F. Najjar, A. Zakhama and P. Horcajada, *Int. J. Pharm.*, 2016, **511**, 1042–1047.

46 P. Horcajada, T. Chalati, C. Serre, B. Gillet, C. Sebrie, T. Baati, J. F. Eubank, D. Heurtaux, P. Clayette, C. Kreuz, J.-S. Chang, Y. K. Hwang, V. Marsaud, P.-N. Bories, L. Cynober, S. Gil, G. Férey, P. Couvreur and R. Gref, *Nat. Mater.*, 2010, **9**, 172–178.

47 F. Boateng and W. Ngwa, *Int. J. Mol. Sci.*, 2020, **21**, 273.

48 M. Levy, N. Luciani, D. Alloyeau, D. Elgrabli, V. Deveaux, C. Pechoux, S. Chat, G. Wang, N. Vats, F. Gendron, C. Factor, S. Lotersztajn, A. Luciani, C. Wilhelm and F. Gazeau, *Biomaterials*, 2011, **32**, 3988–3999.

49 D. K. Mishra, V. Pandey, R. Maheshwari, P. Ghode and R. K. Tekade, in *Basic Fundamentals of Drug Delivery*, ed. R. K. Tekade, Academic Press, 2019, pp. 595–650.

50 H. Marwah, T. Garg, A. K. Goyal and G. Rath, *Drug Delivery*, 2016, **23**, 564–578.

51 N. Davies, D. Hovdal, N. Edmunds, P. Nordberg, A. Dahlén, A. Dabkowska, M. Y. Arteta, A. Radulescu, T. Kjellman, A. Höijer, F. Seeliger, E. Holmedal, E. Andihn, N. Bergenhem, A.-S. Sandinge, C. Johansson, L. Hultin, M. Johansson, J. Lindqvist, L. Björsson, Y. Jing, S. Bartesaghi, L. Lindfors and S. Andersson, *Mol. Ther.–Nucleic Acids*, 2021, **24**, 369–384.

52 T. W. Prow, J. E. Grice, L. L. Lin, R. Faye, M. Butler, W. Becker, E. M. T. Wurm, C. Yoong, T. A. Robertson, H. P. Soyer and M. S. Roberts, *Adv. Drug Delivery Rev.*, 2011, **63**, 470–491.

53 M. de J. Velásquez-Hernández, M. Linares-Moreau, E. Astria, F. Carraro, M. Z. Alyami, N. M. Khashab, C. J. Sumby, C. J. Doonan and P. Falcaro, *Coord. Chem. Rev.*, 2021, **429**, 213651.

54 J. Schubert and M. Chanana, *Curr. Med. Chem.*, 2019, **25**, 4556–4586.

55 E. Lu, S. Li and Z. Wang, *Asian J. Pharm. Sci.*, 2017, **12**, 9–20.

56 I. L. Bergin and F. A. Witzmann, *Int. J. Biomed. Nanosci. Nanotechnol.*, 2013, **3**, DOI: 10.1504/IJBNN.2013.054515.

57 N. R. Yacobi, F. Fazllolahi, Y. H. Kim, A. Sipos, Z. Borok, K.-J. Kim and E. D. Crandall, *Air Qual., Atmos. Health*, 2011, **4**, 65–78.

58 H. G. Preuss, *Clin. Lab. Med.*, 1993, **13**, 103–116.

59 E. Moutzouri, E. N. Liberopoulos and M. Elisaf, *Arch. Med. Sci.*, 2011, **7**, 736–739.

60 K. E. Barrett, S. Boitano and S. M. Barman, *Ganong's Review of Medical Physiology*, McGraw-Hill Professional Publishing, New York, USA, 23rd edn, 2010.

61 S. Bonvalot, P. L. Rutkowski, J. Thariat, S. Carrère, A. Ducassou, M.-P. Sunyach, P. Agoston, A. Hong, A. Mervoyer, M. Rastrelli, V. Moreno, R. K. Li, B. Tiangco, A. C. Herraez, A. Gronchi, L. Mangel, T. Sy-Ortin, P. Hohenberger, T. de Baère, A. Le Cesne, S. Helfre, E. Saada-Bouzid, A. Borkowska, R. Anghel, A. Co, M. Gebhart, G. Kantor, A. Montero, H. H. Loong, R. Vergés, L. Lapeire, S. Dema, G. Kacso, L. Austen, L. Moureau-Zabotto, V. Servois, E. Wardelmann, P. Terrier, A. J. Lazar, J. V. M. G. Bovée, C. Le Péchoux and Z. Papai, *Lancet Oncol.*, 2019, **20**, 1148–1159.

62 P. C. Trivedi, J. J. Bartlett and T. Pulinilkunnil, *Cells*, 2020, **9**, 1131.

63 M. Johannsen, B. Thiesen, P. Wust and A. Jordan, *Int. J. Hyperth. Off. J. Eur. Soc. Hyperthermic Oncol. North Am. Hyperth. Group*, 2010, **26**, 790–795.

64 H. Kettiger, A. Schipanski, P. Wick and J. Huwyler, *Int. J. Nanomed.*, 2013, **8**, 3255–3269.

65 D. Schmaljohann, *Adv. Drug Delivery Rev.*, 2006, **58**, 1655–1670.

66 S. Ohkuma and B. Poole, *Proc. Natl. Acad. Sci. U. S. A.*, 1978, **75**, 3327–3331.

67 Y.-B. Hu, E. B. Dammer, R.-J. Ren and G. Wang, *Transl. Neurodegener.*, 2015, **4**, 18.

68 P. Watson, A. T. Jones and D. J. Stephens, *Adv. Drug Delivery Rev.*, 2005, **57**, 43–61.

69 C. Settembre, A. Fraldi, D. L. Medina and A. Ballabio, *Nat. Rev. Mol. Cell Biol.*, 2013, **14**, 283–296.

70 A. Curcio, A. V. de Walle, E. Benassai, A. Serrano, N. Luciani, N. Menguy, B. B. Manshian, A. Sargsian, S. Soenen, A. Espinosa, A. Abou-Hassan and C. Wilhelm, *ACS Nano*, 2021, **15**, 9782–9795.

71 T. G. Meijer, K. A. Naipal, A. Jager and D. C. van Gent, *Future Sci. OA*, 2017, **3**, FSO190.

72 P. Wick, S. Chortarea, O. T. Guenat, M. Roesslein, J. D. Stucki, S. Hirn, A. Petri-Fink and B. Rothen-Rutishauser, *Eur. J. Nanomed.*, 2015, **7**, 169–179.

73 C. M. Leung, P. de Haan, K. Ronaldson-Bouchard, G.-A. Kim, J. Ko, H. S. Rho, Z. Chen, P. Habibovic, N. L. Jeon, S. Takayama, M. L. Shuler, G. Vunjak-Novakovic, O. Frey, E. Verpoorte and Y.-C. Toh, *Nat. Rev. Methods Primers*, 2022, **2**, 1–29.

74 C. Jubelin, J. Muñoz-Garcia, L. Griscom, D. Cochonneau, E. Ollivier, M.-F. Heymann, F. M. Vallette, L. Oliver and D. Heymann, *Cell Biosci.*, 2022, **12**, 155.

75 M. Kapałczyńska, T. Kolenda, W. Przybyła, M. Zajączkowska, A. Teresiak, V. Filas, M. Ibbs, R. Bliźniak, Ł. Łuczewski and K. Lamperska, *Arch. Med. Sci.*, 2018, **14**, 910–919.

76 Y. Imamura, T. Mukohara, Y. Shimono, Y. Funakoshi, N. Chayahara, M. Toyoda, N. Kiyota, S. Takao, S. Kono, T. Nakatsura and H. Minami, *Oncol. Rep.*, 2015, **33**, 1837–1843.

77 M. Viceconti, F. Pappalardo, B. Rodriguez, M. Horner, J. Bischoff and F. Musuamba Tshinanu, *Methods*, 2021, **185**, 120–127.

78 M. de J. Velásquez-Hernández, R. Ricco, F. Carraro, F. Ted Limpoco, M. Linares-Moreau, E. Leitner, H. Wiltsche, J. Rattenberger, H. Schröttner, P. Frühwirt, E. M. Stadler, G. Gescheidt, H. Amenitsch, C. J. Doonan and P. Falcaro, *CrystEngComm*, 2019, **21**, 4538–4544.

79 A. Malysheva, A. Ivask, C. L. Doolette, N. H. Voelcker and E. Lombi, *Nat. Nanotechnol.*, 2021, **16**, 926–932.

80 L. Wang, T. Zhang, P. Li, W. Huang, J. Tang, P. Wang, J. Liu, Q. Yuan, R. Bai, B. Li, K. Zhang, Y. Zhao and C. Chen, *ACS Nano*, 2015, **9**, 6532–6547.

81 X. Jiang, T. Miclăuş, L. Wang, R. Foldbjerg, D. S. Sutherland, H. Autrup, C. Chen and C. Beer, *Nanotoxicology*, 2015, **9**, 181–189.

82 A. Balfourier, N. Luciani, G. Wang, G. Lelong, O. Ersen, A. Khelfa, D. Alloyeau, F. Gazeau and F. Carn, *Proc. Natl. Acad. Sci. U. S. A.*, 2020, **117**, 103–113.

83 A. M. Nowicka, U. Hasse, M. Hermes and F. Scholz, *Angew. Chem., Int. Ed.*, 2010, **49**, 1061–1063.

84 J. Modrzynska, T. Berthing, G. Ravn-Haren, K. Kling, A. Mortensen, R. R. Rasmussen, E. H. Larsen, A. T. Saber, U. Vogel and K. Loeschner, *PLoS One*, 2018, **13**, e0202477.

85 U. M. Graham, M. T. Tseng, J. B. Jasinski, R. A. Yokel, J. M. Unrine, B. H. Davis, A. K. Dozier, S. S. Hardas, R. Sultana, E. A. Grulke and D. A. Butterfield, *ChemPlusChem*, 2014, **79**, 1083–1088.

86 G. Chen, Y. Zhang, D. Huang, Y. Liu, C. Li and Q. Wang, *Nano Today*, 2022, **44**, 101504.

87 M. Cao, R. Cai, L. Zhao, M. Guo, L. Wang, Y. Wang, L. Zhang, X. Wang, H. Yao, C. Xie, Y. Cong, Y. Guan, X. Tao, Y. Wang, S. Xu, Y. Liu, Y. Zhao and C. Chen, *Nat. Nanotechnol.*, 2021, **16**, 708–716.

88 A. V. de Walle, A. P. Sangnier, A. Abou-Hassan, A. Curcio, M. Hémadi, N. Menguy, Y. Lalatonne, N. Luciani and C. Wilhelm, *Proc. Natl. Acad. Sci. U. S. A.*, 2019, **116**, 4044–4053.

89 F. Mazuel, A. Espinosa, N. Luciani, M. Reffay, R. Le Borgne, L. Motte, K. Desboeufs, A. Michel, T. Pellegrino, Y. Lalatonne and C. Wilhelm, *ACS Nano*, 2016, **10**, 7627–7638.

90 L. Gutiérrez, S. Romero, G. B. da Silva, R. Costo, M. D. Vargas, C. M. Ronconi, C. J. Serna, S. Veintemillas-Verdaguer and M. del Puerto Morales, *Biomed. Eng. Biomed. Tech.*, 2015, **60**, 417–425.

91 Y. Javed, L. Lartigue, P. Hugounenq, Q. L. Vuong, Y. Gossuin, R. Bazzi, C. Wilhelm, C. Ricolleau, F. Gazeau and D. Alloyeau, *Small*, 2014, **10**, 3325–3337.

92 G. Veronesi, M. Moros, H. Castillo-Michel, L. Mattera, G. Onorato, K. D. Wegner, W. L. Ling, P. Reiss and C. Tortiglione, *ACS Appl. Mater. Interfaces*, 2019, **11**, 35630–35640.

93 X. He, Y. Pan, J. Zhang, Y. Li, Y. Ma, P. Zhang, Y. Ding, J. Zhang, Z. Wu, Y. Zhao, Z. Chai and Z. Zhang, *Environ. Pollut.*, 2015, **196**, 194–200.

94 À. Ruyra, A. Yazdi, J. Espín, A. Carné-Sánchez, N. Roher, J. Lorenzo, I. Imaz and D. Maspoch, *Chem. – Eur. J.*, 2015, **21**, 2508–2518.

95 L. Cooper, T. Hidalgo, M. Gorman, T. Lozano-Fernández, R. Simón-Vázquez, C. Olivier, N. Guillou, C. Serre, C. Martineau, F. Taulelle, D. Damasceno-Borges, G. Maurin, Á. González-Fernández, P. Horcajada and T. Devic, *Chem. Commun.*, 2015, **51**, 5848–5851.

96 X. Li, L. Lachmanski, S. Safi, S. Sene, C. Serre, J. M. Grenèche, J. Zhang and R. Gref, *Sci. Rep.*, 2017, **7**, 1–11.

97 I. Bezverkhyy, G. Weber and J.-P. Bellat, *Microporous Mesoporous Mater.*, 2016, **219**, 117–124.

98 E. Bellido, M. Guillevic, T. Hidalgo, M. J. Santander-Ortega, C. Serre and P. Horcajada, *Langmuir*, 2014, **30**, 5911–5920.

99 J. Yang, X. Chen, Y. Li, Q. Zhuang, P. Liu and J. Gu, *Chem. Mater.*, 2017, **29**, 4580–4589.

100 I. Abánades Lázaro, S. Haddad, S. Sacca, C. Orellana-Tavra, D. Fairen-Jimenez and R. S. Forgan, *Chem*, 2017, **2**, 561–578.

101 K. Liang, R. Ricco, C. M. Doherty, M. J. Styles, S. Bell, N. Kirby, S. Mudie, D. Haylock, A. J. Hill, C. J. Doonan and P. Falcaro, *Nat. Commun.*, 2015, **6**, 1–8.

102 Z. Ahmad, *Principles of Corrosion Engineering and Corrosion Control*, Elsevier, 2006.

103 J. J. Patricia and A. S. Dhamoon, in *StatPearls*, StatPearls Publishing, Treasure Island, FL, 2022.

104 S. Phang-Lyn and V. A. Llerena, in *StatPearls*, StatPearls Publishing, Treasure Island, FL, 2022.

105 V. E. Del Bene, in *Clinical Methods: The History, Physical, and Laboratory Examinations*, ed. H. K. Walker, W. D. Hall and J. W. Hurst, Butterworths, Boston, 3rd edn, 1990.

106 S. Feng, X. Zhang, D. Shi and Z. Wang, *Front. Chem. Sci. Eng.*, 2021, **15**, 221–237.

107 J. Hermannsdörfer, N. de Jonge and A. Verch, *Chem. Commun.*, 2015, **51**, 16393–16396.

108 E. G. Heckert, S. Seal and W. T. Self, *Environ. Sci. Technol.*, 2008, **42**, 5014–5019.

109 T. Finkel and N. J. Holbrook, *Nature*, 2000, **408**, 239–247.

110 J. M. McCord and I. Fridovich, *J. Biol. Chem.*, 1969, **244**, 6049–6055.

111 A. Nandi, L.-J. Yan, C. K. Jana and N. Das, *Oxid. Med. Cell. Longevity*, 2019, **2019**, e9613090.

112 A. Deisseroth and A. L. Dounce, *Physiol. Rev.*, 1970, **50**, 319–375.

113 C. M. C. Andrés, J. M. Pérez de la Lastra, C. A. Juan, F. J. Plou and E. Pérez-Lebeña, *Stresses*, 2022, **2**, 256–274.

114 R. W. Tarnuzzer, J. Colon, S. Patil and S. Seal, *Nano Lett.*, 2005, **5**, 2573–2577.

115 J. A. Imlay, S. M. Chin and S. Linn, *Science*, 1988, **240**, 640–642.

116 K. D. Sugden, R. D. Geer and S. J. Rogers, *Biochemistry*, 1992, **31**, 11626–11631.

117 J. L. Elechiguerra, L. Larios-Lopez, C. Liu, D. Garcia-Gutierrez, A. Camacho-Bragado and M. J. Yacaman, *Chem. Mater.*, 2005, **17**, 6042–6052.

118 R. Kaegi, A. Voegelin, C. Ort, B. Sinnet, B. Thalmann, J. Krismer, H. Hagendorfer, M. Elumelu and E. Mueller, *Water Res.*, 2013, **47**, 3866–3877.

119 A. Wamucho, J. M. Unrine, T. J. Kieran, T. C. Glenn, C. L. Schultz, M. Farman, C. Svendsen, D. J. Spurgeon and O. V. Tsyusko, *Environ. Pollut.*, 2019, **254**, 113078.

120 M. Li, J. Li, J. Sun, Y. He, P. Chen and C. Zhang, *Environ. Sci. Nano*, 2019, **6**, 3611–3624.

121 W.-R. Li, T.-L. Sun, S.-L. Zhou, Y.-K. Ma, Q.-S. Shi, X.-B. Xie and X.-M. Huang, *Int. Biodeterior. Biodegrad.*, 2017, **123**, 304–310.

122 Y. Y. Hong Hu, *J. Microb. Biochem. Technol.*, 2015, **7**, 228–233.

123 F. F. Larese, F. D'Agostin, M. Crosera, G. Adami, N. Renzi, M. Bovenzi and G. Maina, *Toxicology*, 2009, **255**, 33–37.

124 Y. Qing, L. Cheng, R. Li, G. Liu, Y. Zhang, X. Tang, J. Wang, H. Liu and Y. Qin, *Int. J. Nanomed.*, 2018, **13**, 3311–3327.

125 M. Rai, A. P. Ingle, I. Gupta and A. Brandelli, *Int. J. Pharm.*, 2015, **496**, 159–172.

126 A. Gogos, B. Thalmann, A. Voegelin and R. Kaegi, *Environ. Sci. Nano*, 2017, **4**, 1733–1741.

127 D. Borisova, H. Möhwald and D. G. Shchukin, *ACS Nano*, 2011, **5**, 1939–1946.

128 T. W. Quadri, L. O. Olasunkanmi, O. E. Fayemi, M. M. Solomon and E. E. Ebenso, *ACS Omega*, 2017, **2**, 8421–8437.

129 K. Ni, G. Lan, C. Chan, B. Quigley, K. Lu, T. Aung, N. Guo, P. La Riviere, R. R. Weichselbaum and W. Lin, *Nat. Commun.*, 2018, **9**, 2351.

130 J. Zhou, M. Kirk, P. Baldo and F. Lu, *Materialia*, 2021, **18**, 101154.

131 F. Lu, Y. Shen, X. Sun, Z. Dong, R. C. Ewing and J. Lian, *Acta Mater.*, 2013, **61**, 2984–2992.

132 T. D. Shen, *Nucl. Instrum. Methods Phys. Res., Sect. B*, 2008, **266**, 921–925.

133 G. M. Cheng, W. Z. Xu, Y. Q. Wang, A. Misra and Y. T. Zhu, *Scr. Mater.*, 2016, **123**, 90–94.

134 K. D. Timmerhaus and T. M. Flynn, *Cryogenic Process Engineering*, Springer Science & Business Media, 2013.

135 C. G. Simon, S. E. Borgos, L. Calzolai, B. C. Nelson, J. Parot, E. J. Petersen, M. Roesslein, X. Xu and F. Caputo, *J. Controlled Release*, 2023, **354**, 120–127.

136 S. Lee, X. Bi, R. B. Reed, J. F. Ranville, P. Herckes and P. Westerhoff, *Environ. Sci. Technol.*, 2014, **48**, 10291–10300.

137 L. Hendriks, A. Gundlach-Graham, B. Hattendorf and D. Günther, *J. Anal. At. Spectrom.*, 2017, **32**, 548–561.

138 X. Tian, H. Jiang, L. Hu, M. Wang, W. Cui, J. Shi, G. Liu, Y. Yin, Y. Cai and G. Jiang, *TrAC, Trends Anal. Chem.*, 2022, **157**, 116746.

139 H. M. Neu, S. A. Alexishin, J. E. P. Brandis, A. M. C. Williams, W. Li, D. Sun, N. Zheng, W. Jiang,

A. Zimrin, J. C. Fink, J. E. Polli, M. A. Kane and S. L. J. Michel, *Mol. Pharm.*, 2019, **16**, 1272–1281.

140 A. A. Bunaciu, E. gabriela Udriştioiu and H. Y. Aboul-Enein, *Crit. Rev. Anal. Chem.*, 2015, **45**, 289–299.

141 C. F. Holder and R. E. Schaak, *ACS Nano*, 2019, **13**, 7359–7365.

142 T. Uusimaeki, T. Wagner, H. G. Lipinski and R. Kaegi, *J. Nanopart. Res.*, 2019, **21**, 1–11.

143 T. Wagner and J. Eglinger, *thorstenwagner/ij-particlesizer Zenodo 2017*.

144 M. Botifoll, I. Pinto-Huguet and J. Arbiol, *Nanoscale Horiz.*, 2022, **7**, 1427–1477.

145 M. M. van Schooneveld, A. Gloter, O. Stephan, L. F. Zagonel, R. Koole, A. Meijerink, W. J. M. Mulder and F. M. F. de Groot, *Nat. Nanotechnol.*, 2010, **5**, 538–544.

146 M. A. Aronova and R. D. Leapman, *MRS Bull.*, 2012, **37**, 53–62.

147 M. Podgórczyk, W. M. Kwiatek, W. M. Zając, J. Dulińska-Litewka, E. Welter and D. Grolimund, *X-Ray Spectrom.*, 2009, **38**, 557–562.

148 A. Levina, A. I. McLeod, A. Pulte, J. B. Aitken and P. A. Lay, *Inorg. Chem.*, 2015, **54**, 6707–6718.

149 C. Sanchez-Cano, D. Gianolio, I. Romero-Canelon, R. Tucoulou and P. J. Sadler, *Chem. Commun.*, 2019, **55**, 7065–7068.

150 H. A. Castillo-Michel, C. Larue, A. E. Pradas del Real, M. Cotte and G. Sarret, *Plant Physiol. Biochem.*, 2017, **110**, 13–32.

151 M. Podgórczyk, W. M. Kwiatek, D. Grolimund and C. Borca, *Radiat. Phys. Chem.*, 2009, **78**, S53–S57.

152 S. L. McArthur, G. Mishra and C. D. Easton, in *Surface Analysis and Techniques in Biology*, ed. V. S. Smentkowski, Springer International Publishing, Cham, 2014, pp. 9–36.

153 H. Mekaru, A. Yoshigoe, M. Nakamura, T. Doura and F. Tamanoi, *ACS Appl. Nano Mater.*, 2019, **2**, 479–488.

154 C.-K. Wu, M. Yin, S. O'Brien and J. T. Koberstein, *Chem. Mater.*, 2006, **18**, 6054–6058.

155 K. B. Lewis and B. D. Ratner, *J. Colloid Interface Sci.*, 1993, **159**, 77–85.

156 M. Kjærvik, M. Ramstedt, K. Schwibbert, P. M. Dietrich and W. E. S. Unger, *Front. Chem.*, 2021, **9**, 666161.

157 A. L. Urbano-Bojorge, N. Félix-González, T. Fernández, F. del Pozo-Guerrero, M. Ramos and J. J. Serrano-Olmedo, *J. Nano Res.*, 2015, **31**, 129–137.

158 M. Škrátek, A. Dvurečenskij, M. Kluknavský, A. Barta, P. Bališ, A. Mičurová, A. Cigáň, A. Eckstein-Andicsová, J. Maňka and I. Bernátová, *Nanomaterials*, 2020, **10**, 1993.

159 C. Birkl, A. M. Birkl-Toeglhofer, C. Kames, W. Goessler, J. Haybaeck, F. Fazekas, S. Ropele and A. Rauscher, *NeuroImage*, 2020, **220**, 117080.